Bifurcation Analysis of a Simple 3D Oscillator and Chaos Synchronization of its Coupled Systems

Tetsushi Ueta[a,*], Akihisa Tamura[b]

[a] *Center for Admin. Info. Tech., The University of Tokushima, Japan*
[b] *Fac. Eng., The University of Tokushima, Japan*

Abstract

Tamaševičius et al. proposed a simple 3d chaotic oscillator for educational purpose. In fact the oscillator can be implemented very easily and it shows typical bifurcation scenario so that it is a suitable training object for introductory education for students. However, as far as we know, no concrete studies on bifurcations or applications on this oscillator have been investigated. In this paper, we make a thorough investigation on local bifurcations of periodic solutions in this oscillator by using a shooting method. Based on results of the analysis, we study chaos synchronization phenomena in diffusively coupled oscillators. Both bifurcation sets of periodic solutions and parameter regions of in-phase synchronized solutions are revealed. An experimental laboratory of chaos synchronization is also demonstrated.

Keywords: chaotic oscillator, bifurcation analysis, synchronization

1. Introduction

Tamaševičius et al. proposed a very simple chaotic circuit for education purpose[1] The main feature which is different from other three dimensional chaotic circuit is utilization of the exponential nonlinearity of a diode, that is, only the Shockley diode equation exhibits a nonlinear effect in the mathematical model of the circuit. Experimentally a Rössler-type chaotic attractor is confirmed. However, although existence of a period-doubling cascade was described in Ref. [1], no detailed bifurcation analyses have been reported.

In this paper, we investigate bifurcation phenomena in the circuit in detail. We firstly reveal all possible local bifurcations of equilibria and limit cycles with 2-parameter bifurcation diagrams computed by using a shooting method[2, 3, 4] based on numerical integration of variational equations. Secondly we discuss an application of this oscillator; chaos synchronization. When we couple these two oscillators by a resistor, then in-phase chaos synchronization is obtained within a reasonable parameter range. We show bifurcation diagrams of the coupled oscillators and specify the chaos synchronization parameter regions in the diagrams. Finally we demonstrate a laboratory experiment of the coupled oscillator exhibiting a stable in-phase chaos synchronization.

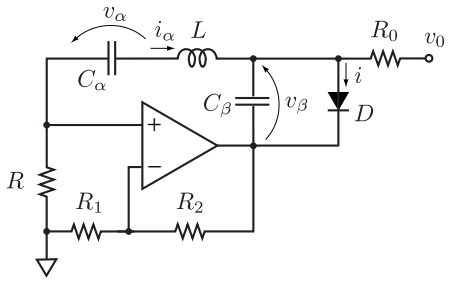

Figure 1: Circuit diagram proposed by Tamaševičius [1].

2. Circuit Model

Figure 1 shows an oscillator proposed by Tamaševičius et al. By referring the formulations in Ref.[1], the circuit equation is as follows:

$$\begin{aligned} C_\alpha \frac{dv_\alpha}{dt} &= i_\alpha \\ L\frac{di_\alpha}{dt} &= \frac{RR_2}{R_1} i_1 - v_\alpha - v_\beta \\ C_\beta \frac{dv_\beta}{dt} &= i_0 + i_\alpha - i \end{aligned} \tag{1}$$

where $i_0 = v_0/R_0$. Here i is the diode current written by Shockley diode equation:

$$i = i_S \left(\exp \frac{ev_\beta}{kT} - 1 \right) \tag{2}$$

where i_S is the saturation current of the reverse direction, e, k, and T are the electron charge, Boltzmann constant, and temperature, respectively. Let us use variable transformations[1]:

$$\begin{aligned} &x = \frac{v_\alpha}{v_x}, \quad y = \frac{\rho i_\alpha}{v_x}, \quad z = \frac{v_\beta}{v_x} \quad v_x = \frac{k}{e}, \\ &\theta = \frac{t}{\tau}, \quad \rho = \sqrt{\frac{L}{C_\alpha}}, \quad \tau = \sqrt{LC_\alpha}, \quad a = \frac{RR_2}{R_1\rho}, \\ &b = \frac{\rho i_0}{v_x}, \quad c = \frac{\rho i_S}{v_x}, \quad \epsilon = \frac{C_\beta}{C_\alpha}, \end{aligned}$$

then we have the following normalized differential equations:

$$\begin{aligned} \dot{x} &= y \\ \dot{y} &= ay - x - z \\ \epsilon \dot{z} &= b + y - c(\exp z - 1) \end{aligned} \tag{3}$$

Figure 2 shows a chaotic attractor presented in Ref. [1] with $a = 0.4$, $b = 20$, $c = 4 \times 10^{-9}$, $\epsilon = 0.13$.

*Corresponding author

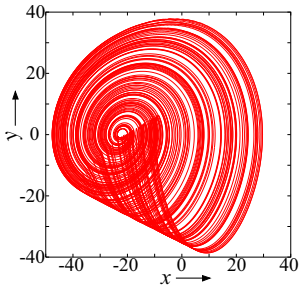

Figure 2: A typical chaotic attractor. A projection to x-y plane.

3. Local Bifurcations

We consistently fix the parameter c since it comes from a physical constant in a diode.

There is a unique equilibrium in Eq. (3); $\boldsymbol{x}_e = (0, -\log(b/c + 1), \log(b/c + 1))$. Only Hopf bifurcation is caused for this equilibrium, and the bifurcation set can be solved analytically.

To track bifurcation sets of periodic solutions, the Poincaré mapping is applied. Suppose the system is described by $\dot{\boldsymbol{x}} = \boldsymbol{f}(\boldsymbol{x})$, where $\boldsymbol{x} = (x, y, z)$, and $\boldsymbol{x}(t) = \boldsymbol{\varphi}(t, \boldsymbol{x}_0)$ be a solution with the initial condition $\boldsymbol{x}(0) = \boldsymbol{x}_0 = \boldsymbol{\varphi}(0, \boldsymbol{x}_0)$. A periodic solution is expressed as $\boldsymbol{x}(t) = \boldsymbol{\varphi}(t + \tau, \boldsymbol{x}_0)$, where τ is the period. We define the Poincaré section for Eq. (3) as $\Pi = \{\boldsymbol{x} \in \boldsymbol{R}^3 \,|\, y = 0\}$, thus the Poincaré mapping T is written as follows:

$$T : \boldsymbol{R}^3 \to \boldsymbol{R}^3; \boldsymbol{x} \mapsto T(\boldsymbol{x}), \boldsymbol{x} \in \boldsymbol{R}^n \tag{4}$$

Thereby the condition of the fixed point is written as $T(\boldsymbol{x}_0) = \boldsymbol{x}_0$. The Jacobian matrix $\partial\boldsymbol{\varphi}/\partial\boldsymbol{x}_0$ is a principal matrix solution obtained by numerical integration of the following variational equation from $t = 0$ to $t = \tau(\boldsymbol{x}_0)$:

$$\frac{d}{dt}\frac{\partial\boldsymbol{\varphi}}{\partial\boldsymbol{x}_0} = \frac{\partial\boldsymbol{f}}{\partial\boldsymbol{x}}\frac{\partial\boldsymbol{\varphi}}{\partial\boldsymbol{x}_0}, \qquad \left.\frac{\partial\boldsymbol{\varphi}}{\partial\boldsymbol{x}_0}\right|_{t=0} = \boldsymbol{I}_3 \tag{5}$$

where $\boldsymbol{I}_3$ is the 3×3 identical matrix. Stability of the fixed point of the Poincaré mapping depends on the roots of the characteristic equation:

$$\chi_\mu = \left|\frac{\partial\boldsymbol{\varphi}}{\partial\boldsymbol{x}_0} - \mu I_3\right| = 0. \tag{6}$$

Suppose that $\boldsymbol{u} \in \Sigma \subset \boldsymbol{R}^2$ is a location on the local coordinate, then there is a projection satisfying $p(\boldsymbol{x}_0) = \boldsymbol{u}_0$. Let $\boldsymbol{u}_1$ be a point on Σ, and $\boldsymbol{\varphi}(t, \boldsymbol{x}_1)$ be the solution starting in $h^{-1}(\boldsymbol{u}_1) = \boldsymbol{x}_1 \in \Pi$. Let also the $\boldsymbol{x}_2 \in \Pi$ be a point at which $\boldsymbol{\varphi}(t, \boldsymbol{x}_1)$ intersects with the return time $\tau(\boldsymbol{x}_1)$, thus we have $\boldsymbol{x}_2 = \boldsymbol{\varphi}(\tau(\boldsymbol{x}_1), \boldsymbol{x}_1)$. Then we define the Poincaré mapping on the local coordinate system:

$$\begin{aligned} T_\ell \quad &: \quad \Sigma \to \Sigma \\ \boldsymbol{u}_1 \quad &\mapsto \quad \boldsymbol{u}_2 = p(\boldsymbol{\varphi}(\tau(h^{-1}(\boldsymbol{u}_1)), p^{-1}(\boldsymbol{u}_1))) \\ &\qquad = p \circ T \circ p^{-1}(\boldsymbol{u}_1) \end{aligned} \tag{7}$$

The fixed point of the mapping T_ℓ is given by:

$$T_\ell(\boldsymbol{u}_0) = \boldsymbol{u}_0. \tag{8}$$

A bifurcation set is tracked by a shooting method, i.e., a bifurcation parameter value is obtained by solving simultaneous equations Eqs. (6) and (8) with Newton's method[2].

In the following subsections, we investigate bifurcations of periodic solutions with variations of parameters a, b, and ϵ. We fix the parameter c consistently as 4×10^{-9}.

3.1. Bifurcations in a-b Plane

Figure 3 is a bifurcation diagram of equilibria and periodic solutions for Eq. (3) in a-b parameter plane. All phenomena given in this diagram is realized by changing values of all resistors, i.e., R, R_0, R_1 and R_2. h is Hopf bifurcation of the equilibrium. With this bifurcation, the diagram is split into two parts; an oscillatory region and a non oscillatory region. Right after getting Hopf bifurcation, a stable equilibrium becomes unstable and we have a stable limit cycle around the equilibrium. Figure 4 (a) illustrates an unstable equilibrium $\boldsymbol{x}_e$, a stable limit cycle, and the fixed point $\boldsymbol{x}_0$ at the point (A) in Fig.3. The period-doubling and tangent bifurcations are labeled by I and G, respectively. The superscription of them indicate the period before the bifurcation.

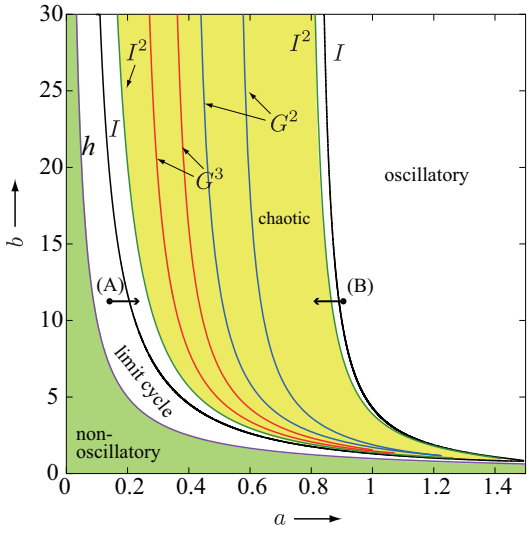

Figure 3: Bifurcation diagram in a-b plane. $\epsilon = 0.13$.

There is an island surrounded by I in oscillatory region. Inside of the island, the period-doubling cascades are developed and then chaotic attractors are obtained. Figures 4(a)–(d) demonstrate this process with parameter variations of a along arrows from (A) and (B) in Fig.3. In a yellow region, we can observe chaotic attractors. There also exist many period-locking regions surrounded by G^k. Figure 5 is an enlarged diagram around chaotic parameter region in Fig. 3. A period-m locking region (window) is edged by G^m and I^m. A stable period-m limit cycle meets a period doubling cascade I^{2m} and eventually becomes a chaotic attractor again. These locking regions are very thin, and they do not overlap each other in a-b plane. At the point (C) in 5, we have a period-three solution, see Fig. 6. These windows tend to be very narrow, thus in the yellow region in Fig. 3, chaotic attractors are abundantly embedded.

Beyond $b > 30$, all bifurcation sets become parallel for b, i.e., the bifurcation structure is insensitive for the value of b.

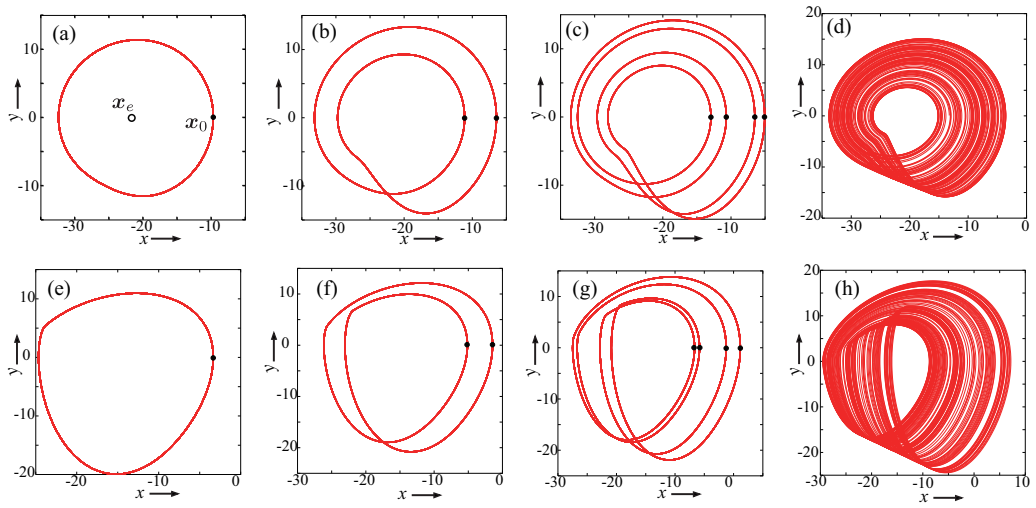

Figure 4: Phase portraits (projections to x-y) with $b = 11.5$. The parameter variation along the arrow from the point (A) in Fig. 3; (a): $a = 0.15$, (b): $a = 0.25$, (c): $a = 0.285$, (d): $a = 0.32$, and along the arrow from the point (B) in Fig. 3; (e): $a = 0.89$, (f): $a = 0.88$, (g): $a = 0.86$, (h): $a = 0.83$.

3.2. Bifurcations in a-ϵ Plane

Figure 7 shows a bifurcation diagram in a-ϵ plane. $b = 15$, $c = 4 \times 10^{-9}$. Similar to Fig.3, the whole region is split into oscillatory and non-oscillatory regions by Hopf bifurcation set h. In the oscillatory region, a fish hook structure[6][7] is formed inside of period-doubling bifurcation set I. That is, two different I^2 curves are overlapped and G^2 in inserted between them.

Both directions shown by arrows from points (A) and from (B) in Fig. 7 exhibit the period-doubling cascade. Phase portraits of the corresponding period-doubling process are shown in Fig. 8. In contrast with Fig. 3, there exists a fish-hook structure[7]. In the chaotic region, there are period-locking regions. G^3 shows a beginning the period-three locking region. The bifurcation diagram is trimmed in $\epsilon \approx 0.8$ and it is not expandable for the small values of ϵ since Eq.(3) is a singular perturbation system, and its solution tends to explode.

3.3. Bifurcations in b-ϵ Plane

The bifurcation structure in b-ϵ is shown in Fig. 9, where $a = 0.9$. In this plane, all phenomena in the diagram are demonstrated by scanning the resistor R_0, and capacitors C_α and C_β.

The structure looks like Fig.7, i.e., non-oscillatory and oscillatory regions are divided by Hopf bifurcation, there are the period-doubling cascades, a fish hook structure, and period-locking regions. The shapes of the corresponding periodic solutions look also similar with Figs. 8.

4. Chaos Synchronization in Coupled Oscillators

As we have revealed that dynamic properties of Tamaševičius circuit by depicting bifurcation diagrams, Tamaševičius circuit is a possible nonlinear oscillation unit which can exhibit a rich variety of attractors by changing parameters. In the following, we call this circuit Tamaševičius oscillator. The next our interest is applications of this circuit.

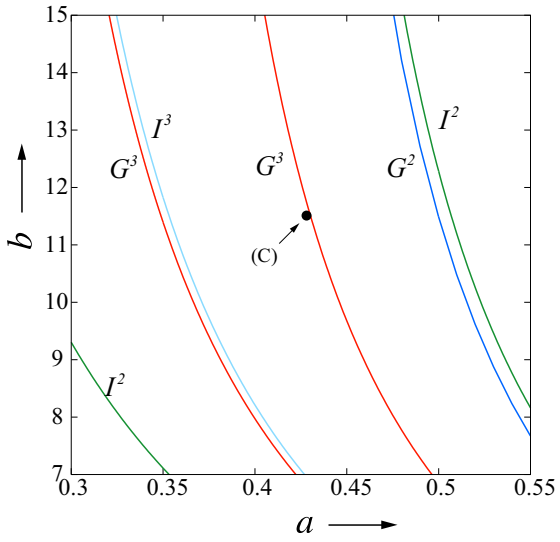

Figure 5: Enlarged bifurcation diagram of Fig. 3.

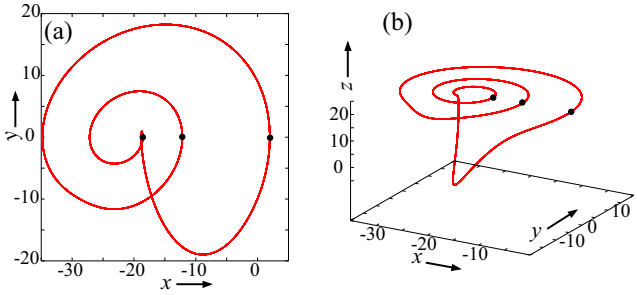

Figure 6: Period-three orbit observed at the point (C) in Fig. 5, $b = 11.5$, (a) $a = 0.431$, a projection to x-y, (b) a 3D vision, $a = 0.35$.

Chaos synchronization attracts much attentions from researchers in nonlinear science[8]. The most successful application of it is secure communication methods[9]. If one has chaotic oscillators which can realize synchronization easily, it is useful for learning chaos synchronization. In this section, we investigate the existence of complete chaos synchronization in diffusively coupled two Tamaševičius oscillators. Our clue of the exploration is bifurcation structures revealed in the previous section.

Let us provide two identical Tamaševičius oscillators. The terminal between L and C_β is chosen as an interface port. Figure 11 shows two Tamaševičius oscillators coupled by a linear conductor R_δ. This kind of diffusive coupling system has an in-phase synchronization of periodic solutions under certain conditions. Since the coupling term is composed by a difference of corresponding variables of oscillators, the in-phase synchronization means vanishment of the coupling. Thus existence of the in-phase synchronization in a diffusive coupling system is confirmed, however, its stability cannot be guaranteed. We specify parameter regions showing stable synchronization with bifurcation diagram.

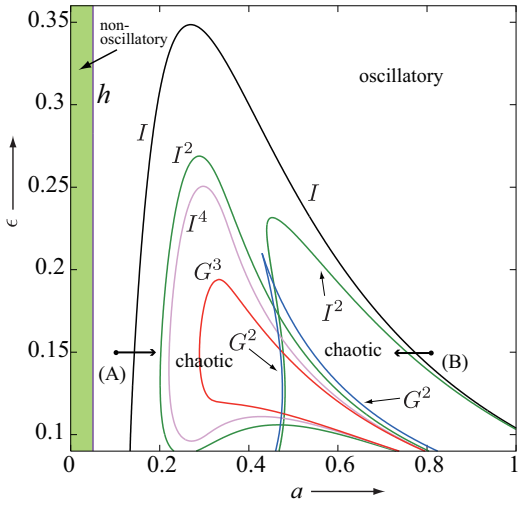

Figure 7: Bifurcation diagram in a-ϵ plane. $b = 15$, $c = 4 \times 10^{-9}$.

Figure 10 shows the coupled Tamaševičius oscillators. The circuit equation is written as follows:

$$\begin{aligned}
C_\alpha \frac{dv_{\alpha 1}}{dt} &= i_{\alpha 1} \\
L \frac{di_{\alpha 1}}{dt} &= \frac{RR_2}{R_1} i_{\alpha 1} - v_{\alpha 1} + v_{\beta 1} \\
C_\beta \frac{dv_{\beta 1}}{dt} &= i_0 + i_{\alpha 1} - i_1 - G_\delta \left(v_{\beta 1} - v_{\beta 2} \right) \\
C_\alpha \frac{dv_{\alpha 2}}{dt} &= i_{\alpha 2} \\
L \frac{di_{\alpha 2}}{dt} &= \frac{RR_2}{R_1} i_{\alpha 2} - v_{\alpha 2} + v_{\beta 2} \\
C_\beta \frac{dv_{\beta 2}}{dt} &= i_0 + i_{\alpha 2} - i_2 - G_\delta \left(v_{\beta 2} - v_{\beta 1} \right)
\end{aligned} \tag{9}$$

Let us try variable transformations as follows:

$$x_j = \frac{v_{\alpha j}}{v_T}, y_j = \frac{\rho i_j}{v_T}, z_j = \frac{v_{\beta j}}{v_T}, j = 1, 2.$$

$$\theta = \frac{t}{\tau}, v_T = \frac{k_B}{e}, \rho = \sqrt{\frac{L}{C_\alpha}}, \tau = \sqrt{LC_\alpha}, a = (k-1)\frac{R}{\rho}, b = \frac{\rho i_0}{v_T}, c = \frac{\rho i_S}{v_T}, \epsilon = \frac{C_\beta}{C_\alpha}, \delta = \frac{\rho}{v_T} G_\delta.$$

Thus we have:

$$\begin{aligned}
\dot{x_1} &= y_1 \\
\dot{y_1} &= a y_1 - x_1 - z_1 \\
\epsilon \dot{z_1} &= b + y_1 - c(\exp z_1 - 1) - \delta(z_1 - z_2) \\
\dot{x_2} &= y_2 \\
\dot{y_2} &= a y_2 - x_2 - z_2 \\
\epsilon \dot{z_2} &= b + y_2 - c(\exp z_2 - 1) - \delta(z_2 - z_1)
\end{aligned} \tag{10}$$

To discuss bifurcations in the coupled system, we take similar way described in Sec. 3. We take $y_1 = 0$ as the Poincaré section, thus the dimension of the local coordinate $\boldsymbol{u}$ is five.

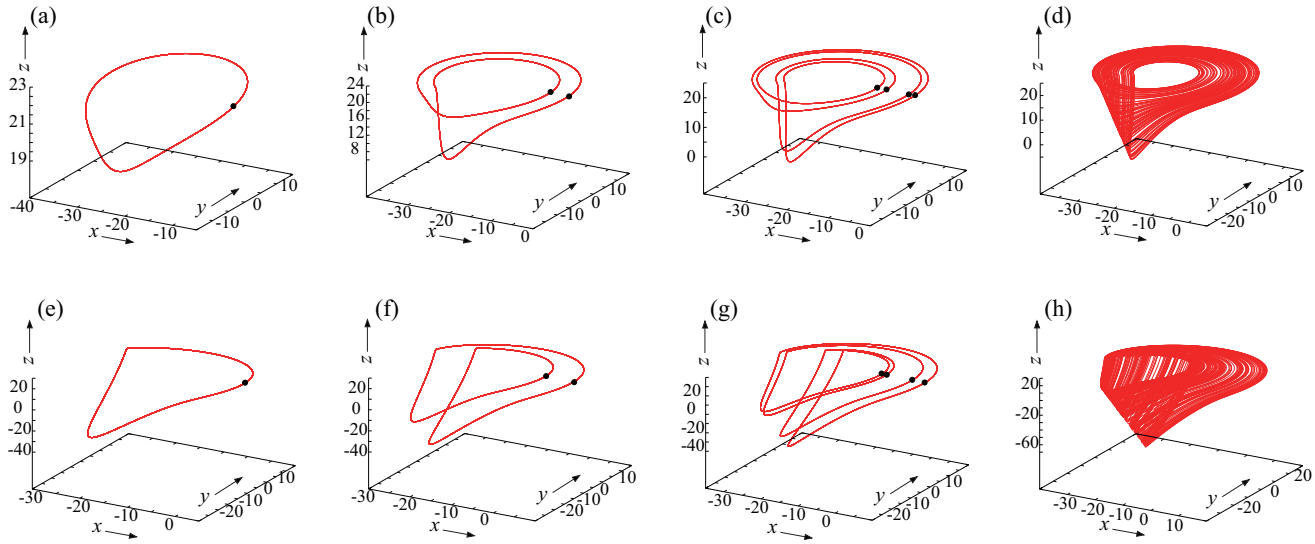

Figure 8: Phase portraits with $\epsilon = 0.15$. The parameter variation along the arrow from the point (A) in Fig. 7; (a): $a = 0.1$, (b): $a = 0.2$, (c): $a = 0.245$, (d): $a = 0.285$, and along the arrow from the point (B); (e): $a = 0.8$, (f): $a = 0.77$, (g): $a = 0.75$, (h): $a = 0.705$.

4.1. Bifurcations in a-δ Plane

Figure 11 shows a bifurcation diagram in a-δ plane for Eq. (10), $b = 11.4$, $c = 4 \times 10^{-9}$, $\epsilon = 0.13$, $\gamma = 1$. By varying R, R_1, R_2, R_d, the whole parameter range shown in this figure can be scanned.

Since both oscillators are identical, there are three cases of synchronization in this system such as symmetric equilibria, synchronized periodic orbits, and chaos synchronization.

The vertical bifurcation lines are corresponding to bifurcation sets (I^k, G^k) occurred when a is scanned along $\epsilon = 0.13$ in Fig. 7. Therefore, chaotic region is roughly identified as the area sectioned by period-doubling cascades of a single oscillator. Inside of the cascade, both synchronized and non-synchronized chaotic attractors could coexist together.

To detect synchronized regions, we evaluate the following discriminant value:

$$\int_{t_0}^{t_1} \|\boldsymbol{x}_1(t) - \boldsymbol{x}_2(t)\| dt < E \tag{11}$$

where $\boldsymbol{x}_i(t) = (x_i(t), y_i(t), z_i(t))$, $i = 1, 2$. We take $E = 0.1$. The integration interval $[t_0, t_1]$ is chosen appropriately, e.g. $[200, 300]$ to remove transitions. The integral tick for the Runge-Kutta method is 0.01. With this discriminant, parameter regions whose attractors satisfying Eq. (11) are regarded as stably synchronized areas. Since there is no general formulation for detecting the edge between synchronized and non-synchronized regions, they should be computed by trial and error. We apply a brute-force method examining Eq (11).

Figure 12 shows phase portraits given by changing parameter a along the arrow from the point (A) in Fig. 11. Initial values with some noise are given appropriately and we obtain attractors after a certain transient time.

The in-phase synchronized attractor observed in the orange region in Fig. 11 gradually lose its synchronicity and may not satisfy the criterion (11). This scenario is coincident to the literature on synchronization, e.g., see Ref. [8]. No local bifurcation is related with this changing. Figure 13 is an example phase portrait of the solution observed at the point (B) in

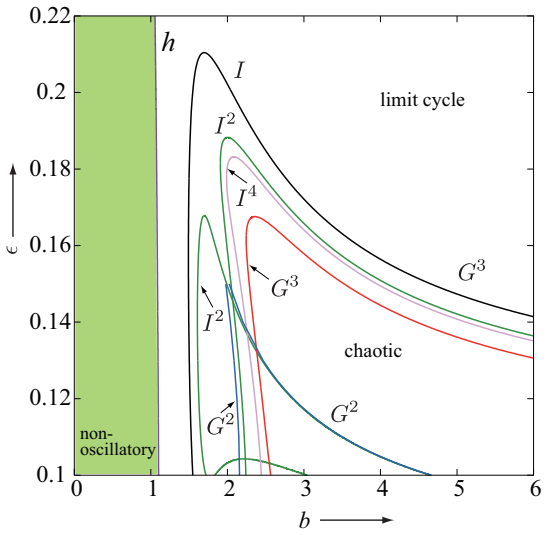

Figure 9: Bifurcation diagram in b-ϵ plane. $a = 0.9$.

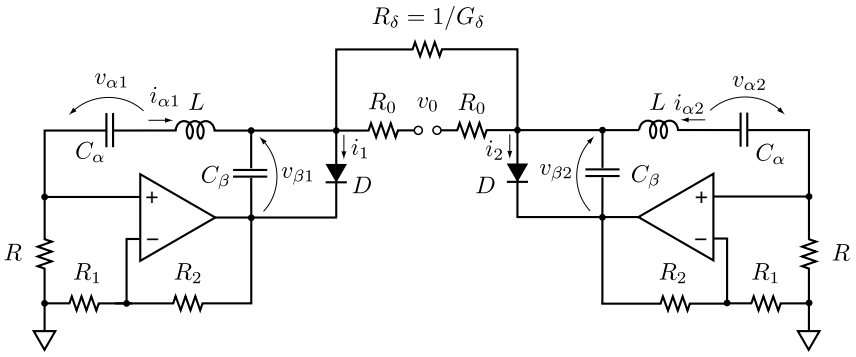

Figure 10: Coupled Tamaševičius oscillators.

Fig. 12. The difference $\boldsymbol{x}_1 and \boldsymbol{x}_2$ does not vanish anymore, i.e., the criterion (11) is not satisfied there, however, the attractors look almost in-phase synchronized.

One exception of this scenario is the period-doubling bifurcation caused around $0.8 < a < 1$. Figure 14 shows an enlargement diagram for Fig.11. Along the direction of arrows, a synchronized period-1 orbit observed inside of the orange region becomes a non-synchronous period-2 orbit outside (the phase difference between z_1 and z_2 is not small). Figure 15 is another enlargement for Fig.11. At the point (D), there is a stable period-2 non-synchronous attractor. By touching the Neimark-Sacker bifurcation[10] labeled by NS^2, a two-reel torus attractor is observed, see Fig. 16. By further changing of a, we have a chaotic attractor via the torus breakdown.

5. Laboratory Experiment of Coupled Oscillator

We demonstrate the coupled Tamaševičius oscillators in a physical laboratory experiment. Circuit elements are chosen as: $L = 100$ mH, $C_\alpha = 100$ nF, $C_\beta = 22$ nF, $R = 1$ kΩ, $R_2 = 10$ kΩ, $R_0 = 20$ kΩ, $R_\delta = 300$ kΩ. These values correspond

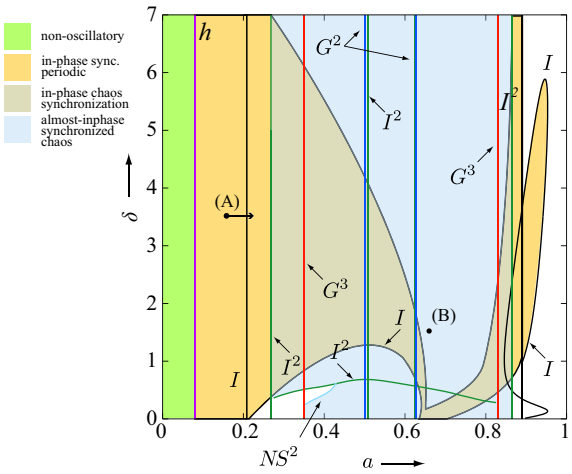

Figure 11: Bifurcation diagram for Eq.(10) in a-δ plane, $b = 11.4$, $c = 4 \times 10^{-9}$, $\epsilon = 0.13$.

approximately the point (A) in Fig. 11. We choose an OP-amp and a diode are LM741 and 1N4148, respectively.

By changing R_2 from 0 to 10 kΩ, we observe the period-doubling cascade of the in-phase synchronized attractors, see Figs. 17. These results show that the chaos synchronization is stably achieved. One of the reasons why that the shape of the attractors differs from the simulations in Fig. 13 is z_i (i.e., $v_{\beta j}$) information is used in 17. But even if x_j-z_j is used for 13, the shape still differs from Fig. 17. The nonlinear characteristics of the diode may not accurately modeled by Shockley equation, however, period-doubling cascades of synchronized attractors are certainly confirmed.

6. Concluding Remarks

We have investigated bifurcation structure of Tamaševičius oscillator in detail. By using a shooting method featuring variational equations accurate bifurcation sets have been traced. Existence of various local bifurcations and chaotic parameter regions have been shown in a-b, a-ϵ, and b-ϵ parameter plane. Typical bifurcation structures including period-doubling cascades, fish hooks have been also confirmed. Next we studied in-phase synchronization of the resistively coupled Tamaševičius oscillators based on bifurcation analysis. A wide in-phase chaos synchronization area has been confirmed in the bifurcation diagram. This means that these oscillators are easy to synchronize. We conclude that the oscillator is suitable for educational purposes including applications of chaos. According to this conclusion, chaos synchronization has been experimentally confirmed in a real circuit implementation of coupled Tamaševičius oscillators.

References

[1] A. Tamaševičius , G. Mykolaitis, V. Pyragas, and K. Pyragas: “A simple chaotic oscillator for educational purposes”, Eur. J. Phys. 26 pp. 61–63, 2005.

[2] T. Ueta, M. Tsueike, H. Kawakami, T. Yoshinaga, Y. Katsuta, “A computation of bifurcation parameter values for limit cycles,” IEICE Trans. Vol. E80, No. 9, pp. 1725–1728, 1997

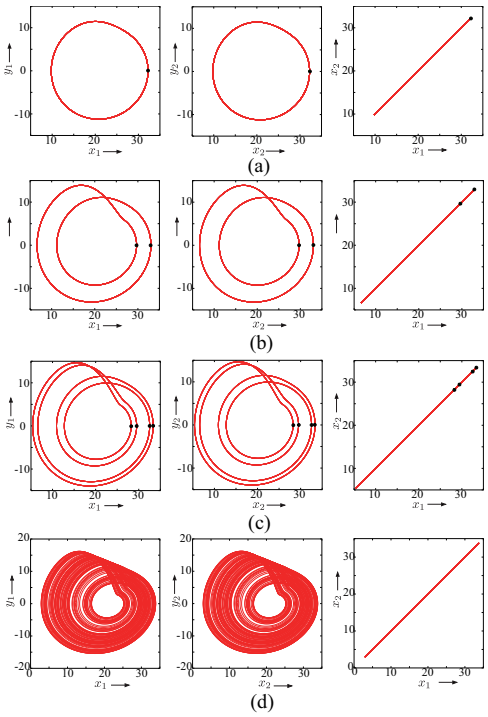

Figure 12: Phase portraits, $\delta = 3.51$. (a): $a = 0.15$, (b): $a = 0.25$, (c):$a = 0.28$, (d): $a = 0.34$. Note that these attractors are started from random initial values.

[3] J. Awrejcewicz, Bifurcation and Chaos in Simple Dynamical Systems, World Scientific, Singapore, 1989.

[4] J. Awrejcewicz, "Numerical investigations of the constant and periodic motions of the human vocal cords including stability and bifurcation phenomena," Dynamics and Stability of Systems Journal, Vol. 5, No. 1, pp. 11–18, 1990.

[5] Y.A. Kuznetsov, Elements of Applied Bifurcation Theory, 2nd. Edition, Springer-Verlag, New York, AMS-112, 1998.

[6] I. Tokuda and R. Tokunaga, "Identification of a parameterized family of chaotic dynamics from time series," in Controlling Chaos and Bifurcation in Engineering Systems, CRC Press, pp. 529–546, 1999.

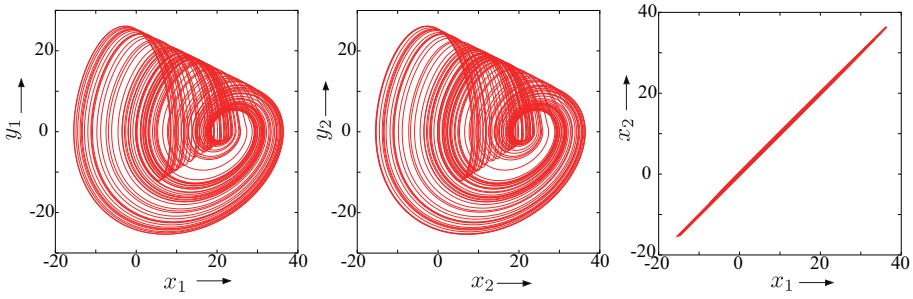

Figure 13: Phase portrait observed at (B) in Fig.13. $a = 0.62$, $\delta = 1.5$. Non-synchronized orbit.

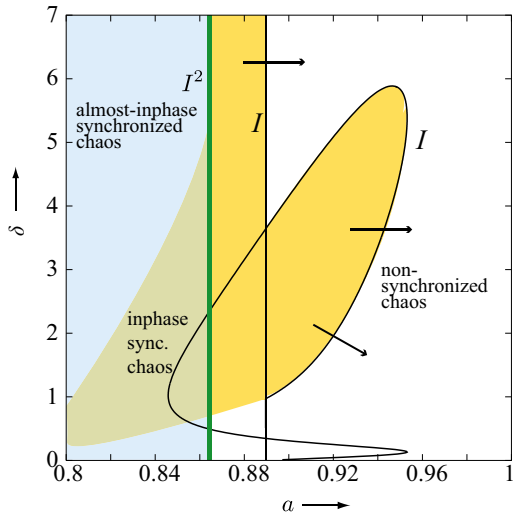

Figure 14: Enlargement of Fig.11.

[7] T. Matsumoto, L.O. Chua, and M. Komuro, "The double scroll," IEEE Trans. Circuits & Syst., CAS-32, No.8, pp.797–818, Aug. 1985.

[8] A. Pikovsky, M. Rosenblum, J. Kurths, Synchronization, Cambridge University Press, New York, 2001.

[9] T. Kapitaniak, Controlling Chaos, Academic Press, 1996.

[10] J. Awrejcewicz, "Bifurcation portrait of the human vocal cord oscillations," Journal of Sound and Vibration, Vol. 136 No. 1, pp. 151–156, 1990.

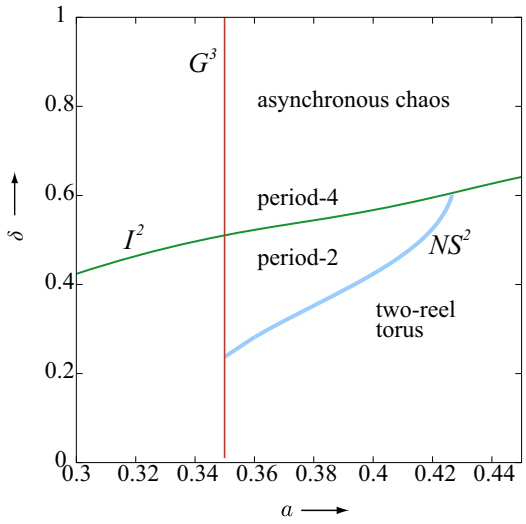

Figure 15: Enlargement of Fig.11.

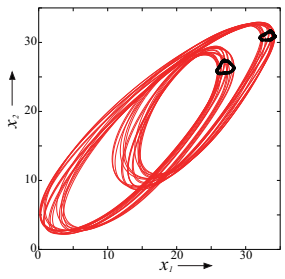

Figure 16: A two-reel torus obtained via Neimark-Sacker bifurcation, $a = 0.41$, $\delta = 0.4$.

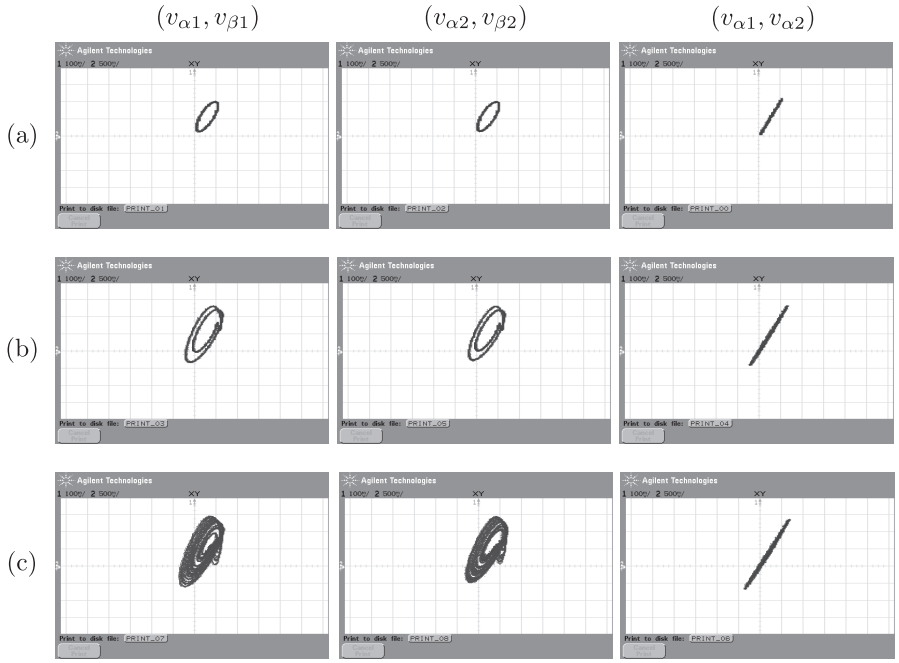

Figure 17: A shot of an oscillograph: in-phase synchronization of attractors. (a): $R_2 = 0\ \Omega$, (b): $R_2 \approx 4\ \mathrm{k}\Omega$, (c): $R_2 \approx 10\ \mathrm{k}\Omega$. Horizontal: 1 V/div. Vertical: 500 mV/div. (a 10:1 attenuator inserted for the horizontal axis.)